Inhibition of PLCβ1 signaling pathway regulates methamphetamine self-administration and neurotoxicity in rats

Xing Xu[1], Runyue Fan[1], Yanqian Ruan[1], Mengjie Xu[1], Jiajie He[1], Mengye Cao[1], Xingxing Li[2], Wenhua Zhou[1], and Yu Liu[1]

[1]Ningbo University Medical School
[2]Ningbo Kangning Hospital

April 28, 2020

Abstract

Background and Purpose: Our previous studies have demonstrated that angiotensin II receptor type 1 (AT1R) in the brain could be a potential treatment for methamphetamine (METH)-induced dependence. The present study aimed to investigate the underlying mechanisms of the inhibitory effect of AT1R on various behavioural effects of METH. Experimental Approach: We first examined the effect of AT1R antagonist, candesartan cilexetil (CAN), on behavioural and neurotoxic effects of METH in vivo and in vitro. We subsequently examine the changes of AT1R and PLCβ1 in vivo and in vitro. Furthermore, we studied the role of PLCβ1 blockade on METH-induced neurotoxicity and synaptic plastic changes. We finally examined the effect of PLCβ1 blockade on the reinforcing and motivational effects of METH. Key Results: CAN significantly elevated METH-induced behavioral dysfunction and neurotoxicity associated with increased oxidative stress. AT1R and phospholipase C β1 (PLCβ1) were significantly upregulated in vivo and in vitro. Inhibition of PLCβ1, effectively alleviated METH-induced neurotoxicity and METH self-administration (SA) by central blockade of the PLCβ1-protein kinase C alpha (PKCα)-cAMP response element-binding protein (CREB) signalling pathway. PLCβ1 blockade significantly decreased the reinforcing and motivation effects of METH. Conclusion and Implications: PLCβ1-PKCα-CREB signalling pathway, as well as a more specific role of PLCβ1, involved the inhibitory effects of CAN on METH-induced behavioural dysfunction and neurotoxicity. Our findings reveal a novel role of PLCβ1 in METH-induced neurotoxicity and METH use disorder.

Ινηιβιτιον οφ ΠΛ^β1 σιγναλινγ πατηωαψ ρεγυλατες μετηαμπηεταμινε σελφ-αδμινιστρατιον ανδ νευροτοξιςιτψ ιν ρατς

Xing Xu[1], Runyue Fan[1], Yanqian Ruan[1], Mengjie Xu[1], Jiajie He[1], Mengye Cao[1], Xingxing Li[2], Wenhua Zhou[1,2, 3], Yu Liu[1*]

[1] Ningbo University School of Medicine, 818 Fenghua Road, Ningbo, Zhejiang 315211, P. R. China

[2] Ningbo Kangning Hospital, 1 South Zhuangyu Road, Ningbo, Zhejiang 315201, P. R. China.

[3] Ningbo Addiction Research and Treatment Center, 21 Xibei Road, Zhejiang 315040, P. R. China

* To whom correspondence should be addressed: liuyu@nbu.edu.cn

Ρυννινγ τιτλε: Τηε Ρολε οφ ΠΛ^β1 ιν METH-ινδυςεδ νευροτοξιςιτψ ανδ ΣΑ

Number of Tables: 0

Number of Figures: 8

Word counts: 5835

Abstract:

Background and Purpose: Our previous studies have demonstrated that angiotensin II receptor type 1 (AT1R) in the brain could be a potential treatment for methamphetamine (METH)-induced dependence. The present study aimed to investigate the underlying mechanisms of the inhibitory effect of AT1R on various behavioural effects of METH.

Experimental Approach: We first examined the effect of AT1R antagonist, candesartan cilexetil (CAN), on behavioural and neurotoxic effects of METH *in vivo and in vitro* . We subsequently examine the changes of AT1R and PLCβ1*in vivo and in vitro* . Furthermore, we studied the role of PLCβ1 blockade on METH-induced neurotoxicity and synaptic plastic changes. We finally examined the effect of PLCβ1 blockade on the reinforcing and motivational effects of METH.

Key Results: CAN significantly elevated METH-induced behavioral dysfunction and neurotoxicity associated with increased oxidative stress. AT1R and phospholipase C beta 1 (PLCβ1) were significantly upregulated in vivo and in vitro. Inhibition of PLCβ1, effectively alleviated METH-induced neurotoxicity and METH self-administration (SA) by central blockade of the PLCβ1-protein kinase C alpha (PKCα)-cAMP response element-binding protein (CREB) signalling pathway. PLCβ1 blockade significantly decreased the reinforcing and motivation effects of METH.

Conclusion and Implications: PLCβ1-PKCα-CREB signalling pathway, as well as a more specific role of PLCβ1, involved the inhibitory effects of CAN on METH-induced behavioural dysfunction and neurotoxicity. Our findings reveal a novel role of PLCβ1 in METH-induced neurotoxicity and METH use disorder.

Key words: methamphetamine, Phospholipase C beta 1, neurotoxicity, cognitive deficits, self-administration

Abbreviations: METH, methamphetamine; RAS, renin–angiotensin system; AT1R, angiotensin II receptor type 1; CAN, candesartan cilexetil; PFC, prefrontal cortex; Hip, hippocampus; PLCβ1, phospholipase C β1; PKCα, protein kinase C alpha; CREB, cAMP response element-binding protein; siRNA, small interfering RNA; SA, self-administration.

What is already known:

Angiotensin II receptor type 1 (AT1R) antagonist, candesartan cilexetil (CAN) effectively reduced METH SA and reinstatement. Furthermore, overexpression of specific miR-219a-5p targeting AT1R regulated METH SA and reinstatement.

What this study adds:

Blockade of AT1R attenuates METH-induced neurotoxicity and cognitive deficits, possibly through the PLCβ1-PKCα-CREB signalling pathway in rats. PLCβ1 blockade significantly decreased METH SA and cue-/drug- reinstatement.

What is the clinical significance:

These results further support the potential utility of PLCβ1 agonist to treat METH use disorder.

Introduction

Long-term METH exposure has been shown to produce a wide range of psychological problems, including psychological distress, depression, suicide, anxiety, violent behaviours, and psychosis(Darke, Kaye, McKetin & Duflou, 2008; Lecomte, Dumais, Dugre & Potvin, 2018; Ma et al., 2018; McKetin, Hides, Kavanagh, Saunders & Dawe, 2018; Potvin, Pelletier, Grot, Hebert, Barr & Lecomte, 2018). Significant cognitive dysfunctions, including attention, prospective memory, retrospective memory, and executive operations, have also been suggested to be associated with long-term use of METH and interfere with daily function (Henry, Minassian & Perry, 2010; Newton, Kalechstein, Duran, Vansluis & Ling, 2004; Rendell, Mazur & Henry, 2009; Simon, Domier, Carnell, Brethen, Rawson & Ling, 2000; Simon, Domier, Sim, Richardson, Rawson & Ling, 2002). In line with the clinical studies, METH administration produces a multitude of behavioural

abnormalities, including object and spatial memory impairments in the animals (Potvin, Pelletier, Grot, Hebert, Barr & Lecomte, 2018; Rogers, De Santis & See, 2008). Neurotoxicity is suggested to be one of the main mechanisms underlying METH-induced cognitive deficits. Exposure to high-dose METH leads to neuronal or glial toxicity in striatum, prefrontal cortex and amygdala in both rats and mice (Mark, Soghomonian & Yamamoto, 2004; Tata & Yamamoto, 2008; Veerasakul, Thanoi, Reynolds & Nudmamud-Thanoi, 2016; Zhu, Xu & Angulo, 2006). These comorbid disorders may further deteriorate the consequences of METH use disorder, indicating the need for "trans-diagnostic treatment approaches" (Bernheim, See & Reichel, 2016; Hartel-Petri et al., 2017). Due to the lack of effective pharmacological treatment for METH use disorder, the medications specifically targeting the improvement of cognitive impairments may be promising to treat METH use disorder (Bernheim, See & Reichel, 2016; Moszczynska & Callan, 2017; Soares & Pereira, 2019; Zhong et al., 2016).

While there is a renin–angiotensin system (RAS) found in most peripheral organs and tissues, there is an independent RAS in the brain. Angiotensin II (Ang II) acts as a neuropeptide, neuromodulator, neurotransmitter, and neurohormone in the central nervous system (CNS) (Bali & Jaggi, 2013). It has been suggested to have a significant impact on several neurological and psychological disorders, such as Huntington's chorea, epilepsy, Alzheimer's disease, Parkinson's disease, and depression (Bali & Jaggi, 2013; Hariharan, Shetty, Shirole & Jagtap, 2014; Kehoe, Al Mulhim, Zetterberg, Blennow & Miners, 2019; Krasniqi & Daci, 2019; Labandeira-Garcia, Rodriguez-Perez, Valenzuela, Costa-Besada & Guerra, 2016; Vian et al., 2017; Wright & Harding, 2019; Wright, Yamamoto & Harding, 2008). Ang II produces different effects by acting on its two receptor subtypes: Ang II type 1 receptor (AT1R) and type 2 receptor (AT2R). The physiological actions of Ang II have been suggested to be mainly mediated through AT1R. For example, blockade of AT1R by losartan reduces the incidence and progression to Alzheimer's disease and mediates cognitive behaviours in mice (Royea, Zhang, Tong & Hamel, 2017). Losartan can also prevent ovariectomy-induced cognitive deficits and anxiety-like behaviour in Long Evans rats (Sharifi, Reisi & Malek, 2019). An AT1R agonist, candesartan cilexetil (CAN), prevents aging-induced memory deficits and cognitive impairment in aged rats (Trofimiuk, Wielgat & Braszko, 2018). Hyperactivation of AT1R in neurons has also been demonstrated to exacerbate cognitive impairment, cell death, and inflammation (Labandeira-Garcia, Rodriguez-Perez, Garrido-Gil, Rodriguez-Pallares, Lanciego & Guerra, 2017). Therefore, AT1R antagonists have been suggested to be a promising therapeutic agent for a number of neurological and psychological disorders(Ivanova & Tchekalarova, 2019).

Due to the high co-morbidity of METH use disorder and psychological disorders, some studies have investigated the role of angiotensin in drug use disorder. Acute and chronic cocaine treatment increases angiotensin converting enzyme (ACE) activity and messenger RNA (mRNA) expression in the striatum and frontal cortex of rats (Visniauskas et al., 2012). ACE inhibitor, captopril, produces analgesic effects and can affect morphine-induced conditioned place preference and withdrawal signs in rats (Alaei & Hosseini, 2007). A growing number of studies have specifically focused the role of Ang II in the behavioural effects of drugs of abuse. For example, repeated METH administration upregulates AT1R mRNA and protein expression in the striatum of mice(Jiang et al., 2018). An AT1R blocker, telmisartan, has shown to attenuate METH-induced hyperlocomotion in mice (Jiang et al., 2018). The interaction between AT1R and amphetamine has been shown to contribute to long-term repeated amphetamine administration in rats (Marchese, Artur de laVillarmois, Basmadjian, Perez, Baiardi & Bregonzio, 2016). In addition, the development of oxidative/inflammatory conditions could be modulated by AT1R in rats exposed to amphetamine (Marchese, Occhieppo, Basmadjian, Casarsa, Baiardi & Bregonzio, 2019).

Our previous studies have also demonstrated that AT1R blockade significantly decreased METH self-administration (SA) and cue-/drug- induced reinstatement, in conjunction with counter-regulation of dopamine receptors and AT1R (Xu et al., 2019). The current study was designed to further explore the mechanism underlying the inhibitory effects of AT1R on the behavioural effects of METH, focusing on the phospholipase C β1 (PLCβ1)-cAMP response element-binding protein (CREB) signalling pathway. Firstly, the effect of AT1R blockade on various behavioural and neurotoxic effects induced by METH was investigated both *in vivo* and *in vitro* . Moreover, the role of PLCβ1-PKC-CREB signalling pathway in the behavioural and neurotoxic

effect of METH was examined. The potential impact of PLCβ1 blockade on the reinforcing and motivational effect of METH was finally studied, using METH SA and drug/cue-induced reinstatement animal model.

Materials and Methods

Drugs

METH was dissolved in 0.9% saline (0.9% NaCl). CAN (TCV-116) was purchased from Tokyo Chemical Industry (Tokyo, Japan) and dissolved in dimethyl sulfoxide (DMSO). U73122 was purchased from Med Chem Express (HY-13419, Shanghai, China). U73122 was dissolved in 20 μl of Tween 20 and resuspended it in saline solution. CAN and U73122 was administered via oral gavage and intraperitoneal (i.p.) injection, respectively.

Animals

Male Sprague-Dawley (SD) rats was purchased from Zhejiang Academy of Medical Sciences, Hangzhou, Zhejiang, China. The animals were individually housed under a standard environment that was previously described(Xu et al., 2019). The experimental protocol was approved by the Institutional Animal Care and Use Committee of Ningbo University. We conducted all the experiments in accordance with the guidelines of the institution.

Body temperature

The rectal temperature was recorded, using a thermometer equipped with a rat rectal probe. The animals were slightly restrained during the testing.

Locomotor activity

Locomotor activity was tracked and recorded, using an automated video tracking system in the recording cages that were made of black Perspex plastic (40 x 40 x 40 cm) with infrared camera above each cage. The detailed procedure for the locomotor activity testing has previously been described (Zhang et al., 2019). In brief, rats moved freely in the chamber for 2 hours per day. Prior to locomotor testing, rats were administered with saline and placed into the locomotor chamber for 4 consecutive days. Locomotor activity was analysed, using behavioural analysis software (AniLab Ltd., Ningbo, China). After each trial, the apparatus was cleaned with 75% ethanol to eliminate any residual odour.

Novel object recognition (NOR) test

The NOR test was carried out in a rectangular open field (120 x 60 x 40 cm) built with white polyvinyl chloride plastic. Prior to the experimental day, rats were placed into the apparatus and allowed to acclimate to it without objects for 6 minutes. On the first experimental day, rats could explore two identical (familiar) objects for 6 minutes. On the second experimental day, a novel object which had a different colour and shape replaced one of familiar objects. Rats were placed in the same arena and allowed to freely explore it for 6 minutes. Exploration was defined as sniffing or touching the objects (no more than 1 cm from the object). If rat sat on or turned the object, it was not considered to be exploratory behaviour. The discrimination index was calculated based on the following equation: discrimination index (%) = (exploration time for novel object/total exploration time for objects) × 100 (%).

Morris water maze (MWM)

The MWM apparatus was equipped with a circular pool (160 cm diameter, 50 cm tall), filled with opaque water (non-toxic white paint, 25 +- 2degC) to cover a platform (Jiang et al., 2016). The pool was arbitrarily divided into north, east, south, and west quadrants. The fixed platform was placed in the east quadrant. The learning phase comprised four consecutives acquisition sessions. Rats were placed in the east quadrant of the maze. Each rat was trained to find the platform with four trials per day. Ras was placed on the platform for 20 s, if it found the platform within the maximum trial time allowed or failed to find the platform within the time limit. Each rat's performance was monitored by a video-tracking camera which

was linked to computer-based image analysis. The latency time (s) was defined as the duration to find the hidden platform during each trial for each session.

Terminal deoxynucleotidyl transferase (TdT) dUTP nick-end labeling (TUNEL)

The TUNEL assay was used to detect apoptotic cells. Apoptosis was determined in the prefrontal cortex (PFC) and hippocampus (Hip) following behavioural tests, according to the manufacturer's instructions (In Situ Cell Death Detection Kit, Roche, USA) (Li et al., 2015). Before staining, tissue sections were deparaffinized and rehydrated. The samples were analysed in five randomly selected high-power fields, using Olympus CX31 microscope (Olympus, Tokyo, Japan). Dark buffy nuclei staining was shown in TUNEL-positive cells, while blue nuclei was observed in TUNEL-negative cells. The total number of TUNEL-positive cells per field was counted and then divided by the field area.

Cell culture and cell viability measurement

Rat pheochromocytoma-derived cells (PC12) and human neuroblastoma cells (SH-SY5Y) were purchased from the Chinese Academy of Sciences (Shanghai, China) and cultured in high glucose modified Eagle's medium (DMEM) that contained 10% fetal bovine serum (FBS), 100 U/ml penicillin, and 100 μg/ml streptomycin at 37°C in a humidified atmosphere of 5% CO_2. The cells were passaged every 2-3 days. The MTT assay (Sigma-Aldrich, St. Louis, MO, USA) was used to measure cell viability. PC12 and SH-SY5Y cells were seeded on 96-well plates and treated with different drugs. A total of 10 μl of MTT solution (5 mg/ml) was added to each well after treatment and the cells was incubated for 4 hours. Subsequently, 100 μl of 10% sodium dodecyl sulfate (SDS) was added to each well and cultured for 16–20 hours. The absorbance of the samples was measured at 570 nm with a reference at 655 nm, using a microplate reader (Thermo Fisher, USA).

Fluorescein diacetate (FDA)/propidium iodide (PI) double staining assay

PC12 and SH-SY5Y cells were seeded on 6-well plates at a density of 1.2×10^6/well. Viable cells contained fluorescein formed from FDA by esterase activity, while non-viable cells were stained by PI as previously described (Wang et al., 2018). The images of each from five randomly selected fields were obtained, in order to quantify cell viability. The average number of FDA-positive cells was calculated, using the following equation: % of cell viability = [number of FDA-positive cells/ (number of PI-positive cells + number of FDA-positive cells)] × 100%.

Measurement of Ang IIlevel and oxidative stress factor levels of rat brain

The levels of AngIIlevel and oxidative stress factor levels (malondialdehyde (MDA), nitric oxide (NO), nicotinamide adenine dinucleotide phosphate (NADPH), glutathione peroxidase (GSH-Px), and superoxide dismutase [SOD]) were determined, using enzyme-linked immunosorbent assay (ELISA) kits (Sigma-Aldrich, St. Louis, Mo, USA) according to the manufacturer's instruction. The absorbance was measured with a microplate reader (Thermo Fisher, USA).

Intracellular reactive oxygen species (ROS) measurement

Intracellular ROS with 2'7'-dichlorodihydrofluorescein diacetate (DCFH-DA, Molecular Probes, Eugene, OR, USA) was measured with a fluorescent dye that can be converted to the membrane impermeable derivative DCFH. The cells were washed with phosphate buffered saline (PBS) and then incubated with 10 μM DCFH-DA at 37°C for 15 minutes. The fluorescence for each well was measured with a plate reader (Wallac, PerkinElmer, Waltham, MA, USA) at 485 nm (excitation) and 525 nm (emission). Images were acquired with a fluorescence microscope (Nikon, Instruments Inc.). SH-SY5Y cells were analysed using the flow cytometry (Cyto FLEX S, Beckman Coulter, Inc, USA) and 20,000 events were acquired per sample. The FL2 channel was used to assess intracellular ROS levels. Flow Jo software were used to analyse cell populations.

Brain tissue collection

Two hours after the behavioural tasks, rats were anesthetized with 30 mg/kg sodium pentobarbital and perfused them with ice-cold saline. The brain was quickly dissected after perfusion. The proteins were isolated in the caudate putamen (CPu), nucleus accumbens (NAc), Hip, PFC, and ventral tegmental area (VTA) and stored at -80°C for further processing.

Western blotting

The western blot procedures are the same as reported previously(Xu et al., 2019). Briefly, brain tissues or SH-SY5Y cells were lysed in an ice-cold mixture of radioimmunoprecipitation assay (RIPA) lysis buffer and a 1:100 dilution of phenylmethylsulfonyl fluoride (PMSF). The homogenates were centrifuged at 13000g for 20 min at 4°C. Protein concentrations were determined with the Pierce BCA protein assay kit (Beyotime Biotechnology, Shanghai, China). Subsequently, equal concentrations of protein samples were diluted by phosphate buffer saline (PBS) and 5x SDS-PAGE loading buffer (Beyotime Biotech Co. Ltd, shanghai, China). Protein samples were loaded onto 10% SDS-PAGE and transferred on polyvinylidene fluoride (PVDF) membranes (Bio-Rad, USA). PVDF membranes were blocked in 5% non-fat dried milk in Tris-buffered saline (TBS) which contained 0.05% Tween 20 for 2 hours. Next, the membranes with the appropriate primary antibody overnight were incubated at 4°C. The following antibodies were used: anti-AT1R (1:1000; ab18801, Abcam), anti-β-actin (1:5000; ab8226, Abcam), anti-PLCβ1 (1:1000; ab182359, Abcam), anti-CREB (1:1000, #9197, Cell Signaling Technology), anti-synaptophysin (SYP,1:1500, #4329, Cell Signaling Technology), anti-post-synaptic density 95 (PSD-95; 1:1500, #3409, Cell Signaling Technology), anti-glucose-regulated protein 78 (GRP78; 1:1000, sc-13539, Santa Cruz), and anti-protein kinase C α (PKCα· 1:1000,sc-8393, Santa Cruz). The membranes were washed with TBST 5 times (8 minutes each) and then incubated them with the corresponding horseradish peroxidase (HRP)-conjugated secondary antibodies at room temperature for 2 hours. Proteins by exposing the membranes were visualized to ECL chemiluminescence reagent (Advansta, Menlo Park, CA, USA). Chemiluminescent Western blot images were detected by a Chemi Scope 6000 Touch (Qinxiang Scientific Instrument Co., Ltd, Shanghai, China) and analyzed integrated peak areas using the Image J software.

Quantitative real-time polymerase chain reaction (qRT-PCR)

Total RNA from METH-treated SH-SY5Y cells were extracted by using the TRIzol reagent. A previously described amplification program was used to reverse transcribed complementary DNA (cDNA) (Dai et al., 2017). Briefly, the purified RNA was reversed using TransScript All-in-One First-Strand cDNA Synthesis SuperMix for qPCR (AT341, TransGen Biotech, Beijing, China). The cDNA was quantified by quantitative reverse transcription-PCR (qRT-PCR) using Trans Start Tip Green qPCR SuperMix (AQ141, TransGen Biotech, Beijing, China). Every reaction was run 3 times and analyzed with the 2^{-Ct} method. Primers were designed by Beijing Genomics institution (Shenzhen, China) and all primer sequences are listed in Supplementary Table S1.

ΠΛ^β1 κνοςκδοων ωιτη σμαλλ ιντερφερινγ PNA (σιPNA) τρανσφεστιον

PLCβ1 siRNA (5'-CACCAUGACAACUGAAAUATT-3') and silencer negative control siRNA (5'-UUCUCCGAACGUGUCAC
3') were designed and purchased from Gene Pharma (Shanghai, China). These siRNAs were transfected into SH-SY5Y cells according to the manufacturer's instructions. siRNAs were dissolved in diethyl pyrocarbonate (DEPC)-treated at a concentration of 20 μM. SH-SY5Y cells were seeded on a 6-well plate. When the cells reached 70% confluence, Lipofectamine 2,000 reagent and 100 nmol siRNA were mixed with Opti-MEM medium. Cells were incubated with siRNAs for 48 h before experimental treatment.

Annexin V apoptosisassay by flow cytometry

Flow cytometry analysis was performed to detect early and late apoptotic cells. According to the instructions of the Annexin V-FITC apoptosis detection kit (AP101, LIANKE, Hangzhou, China), SH-SY5Y cells were seeded on 6-well plates at a density of 6×10^5/well. Cells were transfected with the SiRNA-PLCβ1 and SiRNA-NC then treated with METH (2.0 mM) for 24 h as described before. Cell suspension was transferred from the plates to the centrifuge tube and stained with Annexin V-FITC. According to the detection kit

instructions. The percentage of apoptotic cells measuring cell apoptosis with flow cytometry (Cyto FLEX S, Beckman Coulter, Inc, USA).

METH SA andcue-/drug-induced reinstatement

The details of surgery and the procedures of METH SA were previously described(Xu et al., 2019). Following acquisition, rats self-administered METH under the fixed ratio (FR1) and progressive ratio (PR) schedule. The sham group was uses as the control. The sham group underwent the same surgery as METH SA rats and daily placed in the SA chamber for 4 hours. After METH SA, the animals firstly underwent 7 days of extinction and abstinence respectively. During the cue-induced reinstatement testing, the light and sound cues were presented in the same manner as those used during METH SA. During drug-induced reinstatement testing, rats were firstly treated with an i.p. injection of METH (10mg/kg) and placed in chambers in which drug-associated light/sound cues were presented. Saline infusions substituted METH infusions during both cue- and drug- reinstatement testing.

Experimental procedures

Experiment 1: the effect of ATR1 blockade by CAN on the behavioral and neurotoxic effects of METH in rats.

The procedures of Experiment 1 are summarized in Fig. 1A. DMSO and CAN was administered 2 hours before all behavioral testing. Saline and METH was given 30 minutes prior to all behavioral testing. During the locomotor adaptation period, the rectal temperature was daily recorded. Based on the distance travelled during the last day of adaptation period, rats were divided into five groups (Saline+10CAN, Saline+DMSO, METH+DMSO, METH+5CAN and METH+10CAN). Immediately before the animals were placed into the locomotor chamber on experimental day 1, the rectal temperature was recorded. Locomotor activity testing was carried out for consecutive 4 days. For NOR testing, rats were randomly divided into additional 5 groups (Saline+10CAN, Saline+DMSO, METH+DMSO, METH+5CAN and METH+10CAN) based on the performance during the training session. Additional 5 groups of animals (Saline+10CAN, Saline+DMSO, METH+DMSO, METH+5CAN and METH+10CAN) underwent MWM testing. All rats receiving NOR testing were decapitated. Brain tissues and blood samples were collected. Tissue sections of Hip and PFC were used to assess apoptosis with TUNEL staining. Ang II and oxidative stress factor (MDA, NO, NADPH, GSH-Px, and SOD) levels in the blood were determined with ELISA kits.

Experiment 2: the effect of ATR1 blockade by CAN on the neurotoxic effects of METH in PC12 cells.

PC12 cells pretreated with 1.0, 3.0, and 10.0 uM CAN and 2.5 mM METH was added 30 minutes afterwards. The percent of cell survival was assessed. Cell viability was measured in additional PC12 cells with initial 10.0 uM CAN and following 2.5 mM METH treatment. Intracellular ROS levels were assessed with DCFH-DA staining.

Εξπεριμεντ 3: τηε εφφεςτ οφ METH ον τηε προτειν εξπρεσσιον οφ AT1P ανδ ΠΛ˜β1 ιν ρατς ανδ ΣH-ΣΨ5Ψ ςελλς.

Rats were randomly divided into two groups (saline vs. METH). Daily i.p. injections of either saline or METH (10 mg/kg/day) were administered for 4 consecutive days. The animals were sacrificed and brain tissues of PFC and Hip were collected. AT1R and PLCβ1 protein expression was measured with western blotting. Additional two groups of rats were randomly divided into Sham and SA-FR1 groups. Following METH SA acquisition, SA-FR1 group (n=12) were maintained on 0.05mg/kg/infusion of METH under the FR1 schedule for 14 days. Daily SA session lasted 4 hours. Following the last SA day, the brain tissues of CPu, PFC, Hip and NAc were collected and PLCβ1 protein expression was examined. Another two groups of rats were randomly divided into Sham and SA-PR groups. The SA-PR group were treated in the same manner as SA-FR1 group, except for the use of PR schedule during METH SA period. SH-SY5Y cells were seeded onto 96-well plates and treated with 0, 0.5, 1.0, 2.0, 2.5, or 3.0 mM METH. The PLCβ1protein and

mRNA levels were subsequently determined. Additional SH-SY5Y cells were treated with 2.5 mM METH. PLCβ1 protein and mRNA levels were measured 0, 2, 4, 5, 16, and 24 hours after METH treatment.

Εξπεριμεντ 4: τηε εφφεςτ οφ ΠΛ˜β1 βλοςκαδε ον METH-ινδυςεδ νευροτοξιςιτψ ιν ΣΗ-ΣΨ5Ψ ςελλς ανδ σψναπτις πλαστιςιτψ ςηανγες.

SH-SY5Y cells were pretreated with 0, 1.0, 3.0, and 10.0 uM U73122 and 2.0 mM METH was added 30 minutes afterwards. The percent of cell survival was subsequently measured. Cell viability was measured in SH-SY5Y cells with initial 3.0 uM U73122 and following 2.0 mM METH treatment. SH-SY5Y cells were transfected with siRNA-PLCβ1 or siRNA-NC, followed by 2.0 mM METH treatment for 24 hours. Apoptotic cells were subsequently measured by flow cytometry. SH-SY5Y cells were treated with 3.0 uM U73122 and subsequent 2.0 mM METH. Intracellular ROS and GRP78 protein levels were assessed with DCFH-DA staining and western blot respectively. SH-SY5Y cells were treated with 3.0 uM U73122 and subsequent 2.0 mM METH. The effect of U73122 on the protein and mRNA expression of PLCβ1, PKCα, and CREB in SH-SY5Y cells was assessed with qRT-PCR and western blotting. Rats was administered U73122 30 minutes prior to Saline and METH for consecutive 4 days. Brain tissue sections of PFC were used to assess the protein expression of SYP and PSD-95 with western blotting.

Εξπεριμεντ 5: Τηε εφφεςτ οφ ΠΛ˜β1 βλοςκαδε βψ Υ73122 ον METH ΣΑ ανδ ςυε-/δρυγ-ινδυςεδ ρεινστατεμεντ οφ METH ΣΑ

The experimental procedure of Experiment 5 is summarized in Fig. 8. Rats were trained to self-administer METH. Based on the average of METH infusions during the last two days of the METH acquisition period, the animals were divided into three groups: METH+saline, METH+3U73122, and METH+10U73122. A dose response curve of METH SA (0.025, 0.05, 0.075, and 0.100 mg/kg/infusion) under the FR1 and PR schedule for all the animals was generated. U73122 (3 and 10 mg/kg) was administered 30 minutes prior to each METH SA session in a random order. Additional rats underwent METH SA following the FR1 schedule for 14 days and were subsequently divided into three groups: METH+saline, METH+3U73122, and METH+10U73122. U73122 or saline was administered 30 minutes before each reinstatement session.

Statistics

Data are presented as mean ± SD. $P < 0.05$ was considered as statistically significant. Body temperature is presented as temperature change from baseline (in °C) and analyzed by one-way analysis of variance (ANOVA) with Bonferroni's *post hoc* multiple comparisons test. For the locomotor activity test, two-way repeated measures ANOVA was used with Bonferroni's *post hoc* multiple comparisons to examine the effect of drug treatment on total distance travelled per session across days. For NOR test, one-way ANOVA was utilized to compare the discrimination index among groups. For MWM test, two-way repeated measures ANOVA was applied with Bonferroni's *post hoc* multiple comparisons to examine the effect of drug treatment on the changes of latency time across days. One-way ANOVA was used to compare the average apoptotic cell density among groups in two different brain regions and compare the percentage of cell survival among groups. One-way ANOVA was applied to examine the effect of drug treatment on the levels of Ang II, MDA, NO, NADPH, GSH-Px, and SOD. One-way ANOVA was used to examine the effect of CAN on percentage of cell survival in METH-treated cells, and compared ROS changes. Independent t-test was used to compare the changes of PLCβ1 and ATR1 expression between saline and METH groups in both Hip and PFC. Independent t-test was applied to examine the effect of METH SA under the FR1 and PR schedule on PLCβ1 protein level in different brain regions. One-way ANOVA was utilized to examine the effect of dose and time of METH treatment on the protein and mRNA levels of PLCβ1 in SH-SY5Y cells. One-way ANOVA was used to examine the effect of U73122 on cell viability and percentage of cell survival in METH-treated cells. One-way ANOVA was applied to compare apoptosis among METH, METH+siRNA-NC, and METH+siRNA-PLCβ1 groups. One-way ANOVA was used to compare ROS changes from the baseline, the SYP and PSD-95 protein levels among saline, METH+saline, and METH+U73122 group. One-way ANOVA was applied to examine the effect of U73122 on the protein expression of PLCβ1, PKCα, and CREB in METH-treated cells. Two-way repeated measure ANOVA with Bonferroni's *post hoc*multiple-comparisons

test was used to study the effects of U73122 on SA performance maintained by different doses of METH under the FR1 and PR schedule. Finally, one-way ANOVA was used to study the effects of U73122 on cue- or drug-induced reinstatement of METH SA.

Results

The effect of ATR1 blockade by CAN on the behavioral effects of METH in rats

One-way ANOVA analysis showed a significant group effect on body temperature changes from the baseline ($F_{(4, 30)} = 7.807$, $p < 0.001$). Further *post hoc* analysis showed that the changes of body temperature of the METH+DMSO group was significantly higher than that of the Saline+DMSO group (Fig. 1B*;* $p < 0.01$). The body temperature changes from the baseline of both METH+5CAN (Fig. 1B*;* $p < 0.01$) and METH+10CAN (Fig. 1B*;* $p < 0.001$) groups were significantly lower than METH+DMSO group. There were no significant differences in body temperature changes from the baseline between the METH+5CAN and METH+10CAN groups (Fig. 1B*;* $p > 0.05$). The body temperature changes from the baseline of neither the METH+5CAN nor the METH+10CAN group were significantly different from that of the Saline+DMSO group (Fig. 1B*;* $p > 0.05$).

Two-way repeated measures ANOVA revealed that there were major treatment ($F_{(4, 8)} = 2070$,$p < 0.001$), day ($F_{(3, 6)} = 4.780$, $p < 0.05$), and treatment × time interaction ($F_{(12, 24)} = 5.642$,$p < 0.001$) effects. Further *post hoc* analysis indicated that there were no significant differences in total distance travelled per session among METH+DMSO, METH+5CAN and METH+10CAN groups on day 1 or 4 (Fig. 1C; $p > 0.05$). On day 2, the locomotor activity of METH+10CAN group was significantly lower than that of the METH+DMSO and METH+5CAN groups (Fig. 1C; $p < 0.01$). The locomotor activity of METH+5CAN group was not significantly different from that of METH+DMSO group (Fig. 1C; $p > 0.05$) on Day 2. On Day 3, both METH+5CAN (Fig. 1C; $p < 0.01$) and METH+10CAN (Fig. 1C; $p < 0.01$) groups exhibited a significant decrease in total distance travelled per session when compared to METH+DMSO group (Fig. 1C; $p < 0.05$).

One-way ANOVA indicated that there were no significant differences in the discrimination index among the test groups during NOR training session (Fig. 1D;$F_{(4,18)} = 0.280$,$p > 0.05$). During the NOR retention session, there was a major group effect on discrimination indexes (Fig. 1D; $F_{(4, 18)} = 10.59$, $p < 0.001$). *Post hoc* analysis showed that the discrimination index of METH+DMSO group was significantly lower than that of Saline+DMSO (Fig. 1D; $p< 0.001$) and METH+10CAN (Fig. 1D; $p < 0.01$) groups. The discrimination index of METH+5CAN group was not significantly different from that of METH+DMSO group (Fig. 1D; $p> 0.05$). The discrimination index of Saline+10CAN group was not significantly different from that of Saline+DMSO group (Fig. 1D;$p > 0.05$).

Two-way repeated measure ANOVA revealed major treatment ($F_{(4, 12)} = 28.18$,$p < 0.001$), time ($F_{(3, 9)} = 121.6$, $p < 0.001$), and treatment x time interaction ($F_{(12, 36)} = 0.7122$, $p < 0.05$) effects during MWM testing. Further *post hoc* testing indicated that the latency was not significantly different among five testing groups on day 1 or 4 (Fig. 1E; $p > 0.05$). On day 2, METH+10CAN group spent significantly less time finding the platform, compared to METH+DMSO (Fig. 1E; $p < 0.01$) and METH+5CAN (Fig. 1E; $p< 0.05$) groups. There were no significant differences between saline+10CAN and saline+DMSO groups on day 2 (Fig. 1E; $p> 0.05$). A similar trend was evident on day 3 (METH+10CAN vs. METH+DMSO, $p < 0.01$; METH+10CAN vs. METH+5CAN,$p < 0.05$; saline+10CAN vs. saline+DMSO, $p > 0.05$).

The effect of ATR1 blockade by CAN on METH-induced neurotoxicity in rats

One-way ANOVA revealed a significant group effect on the percentage of apoptotic cells per unit area in PFC (Fig. 2F; $F_{(4, 20)} = 185.9$, $p< 0.001$) and Hip (Fig. 2L; $F_{(4,20)} = 242.061$, $p < 0.001$) of rats. Further *post hoc*analysis showed that METH+DMSO produced a significant increase in the percentage of apoptotic cell per unit area in PFC (Fig. 2F; $p< 0.001$) and Hip (Fig. 2L; $p < 0.001$), compared with Saline+DMSO group. Both METH+5CAN and METH+10CAN groups showed a significantly lower percentage of apoptotic cell per unit area than that of METH+DMSO group in both PFC (Fig. 2F; $p < 0.001$) and Hip (Fig. 2L; p

< 0.001).

One-way ANOVA indicated that there was a significant effect of group for Ang II ($F_{(4, 70)} = 12.49$, $p < 0.001$)), MDA ($F_{(4, 70)} = 13.80$, $p < 0.001$), NO ($F_{(4, 70)} = 8.705$, $p < 0.001$), NADPH ($F_{(4, 70)} = 6.439$, $p < 0.001$), GSH-Px ($F_{(4, 70)} = 13.80$, $p < 0.001$) and SOD ($F_{(4, 70)} = 7.468$, $p < 0.001$). Further *post hoc*analysis revealed that levels of Ang II, MDA, NO, and NADPH were significantly higher in METH+DMSO than those in Saline+DMSO group (Fig. 2M-I; $p < 0.01$). In contrast, central GSH-Px and SOD levels were significantly lower in METH+DMSO than Saline+DMSO group (Fig. 2Q, 2F; $p < 0.01$). The central level of Ang II was significantly decreased in METH+5CAN group, compared with METH+DMSO group (Fig. 2M, $p < 0.01$). The central level of all five tested oxidative stress factors in METH+5CAN group was not significantly different from METH+DMSO group ($p > 0.05$). Administration of 10 mg/kg CAN markedly reversed the increased centrals level of Ang II, MDA, NO, and NADPH induced by METH (Fig. 2M-P;$p < 0.01$). The central levels of GSH-Px and SOD were significantly increased in METH+10CAN group, compared with METH+DMSO group (Fig. 2Q, 2I; $p < 0.01$).

The effect of ATR1 blockade by CAN on the neurotoxic effects of METH in PC12 cells

One-way ANOVA indicated that there was significant group effect on the percentage of cell survival in pre-treatment with various dose of CAN and 2.5 mM METH-treated PC12 cells ($F_{(4, 17)} = 49.99$, $p < 0.001$).The percentage of cell survival was significantly increased by 3.0 μM CAN (Fig. 3A; $p < 0.001$) and 10 μM CAN (Fig. 3A; $p < 0.001$) pre-treatment. Such an effect was absent in METH-treated cells that received 1.0 μM CAN (Fig. 3A; $p > 0.05$). Exposure to 2.5 mM METH significantly decreased cell viability compared to the control group, but pre-treatment of 10 μM CAN significantly increased the number of FDA-labelled and PI-labelled cells treated with METH (Fig. 3B). As shown in Fig. 3C, METH significantly increased intracellular levels of ROS in PC12 cells compared with the control group ($p < 0.001$). Moreover, 10.0 μM CAN significantly reversed the increased intracellular ROS levels induced by 2.5 mM METH ($p < 0.001$).

Τηε εφφεςτ οφ METH ον AT1P ανδ ΠΛ˜β1 προτειν εξπρεσσιον ιν ρατς ανδ ΣΗ-ΣΨ5Ψ ςελλς

Independent t-tests indicated that AT1R and PLCβ1 protein expression was significantly increased in PFC (Fig. 4A; AT1R,$t_{(4)} = 4.863$, $p < 0.01$; PLCβ1,$t_{(4)} = 7.277$, $p < 0.01$) and Hip (Fig. 4B; AT1R, $t_{(4)} = 33.05$, $p < 0.001$; PLCβ1, $t_{(4)} = 28.48$, $p < 0.001$) of rats receiving daily injections of METH. There was a significant increase in PLCβ1 protein expression in the PFC, NAc, and Hip of METH SA rats maintained under FR1 schedule, compared with the sham group (Fig. 4C; PFC, $t_{(4)} = 7.392$, $p < 0.01$; NAc, $t_{(4)} = 13.45$, $p < 0.01$; Hip, $t_{(4)} = 8.414$, $p < 0.01$). A similar effect was evident in PFC and Hip of METH SA rats maintained under PR schedule (Fig. 4D, PFC,$t_{(8)} = 7.713$, $p < 0.001$; Fig. 4E, Hip, $t_{(8)} = 2.784$, $p < 0.05$).

In SH-SY5Y cells, METH significantly increased PLCβ1 protein and mRNA expression in a dose-dependent (Fig. 4F; $F_{(5, 12)} = 657.5$,$p < 0.001$; Fig. 4G; $F_{(5, 6)} = 28.26$, $p < 0.001$) and time-dependent (Fig. 4H;$F_{(5, 12)} = 164.4$, $p < 0.001$; Fig. 4I; $F_{(5, 6)} = 49.56$, $p < 0.001$) manner. Further *post hoc* analysis revealed that PLCβ1 protein expression was significantly higher in 2.0, 2.5, and 3.0 mM METH-treated cells, compared to the control, 0.5, and 1.0 mM METH-treated cells (Fig. 4F; $p < 0.001$). PLCβ1 mRNA expression was significantly increased by 1.0, 2.0, 2.5, and 3.0 mM METH, compared to the control cells (Fig. 4G, $p < 0.001$). Following exposure to 2.0 mM METH for 0, 2, 4, 8, 16, or 24 hours, PLCβ1 protein and mRNA expression were significantly higher than that of the control group (Fig. 4H, 4I, $p < 0.05$).

Τηε εφφεςτ οφ ΠΛ˜β1 βλοςκαδε βψ Υ73122 ανδ ΣιRNA-ΠΛ˜β1 ον METH-ινδυςεδ νευροτοξιςιτψ ιν ΣΗ-ΣΨ5Ψ ςελλς

One-way ANOVA revealed that there was a major group effect on SH-SY5Y cell viability ($F_{(4, 25)} = 25.58$, $p < 0.001$). U73122 dose-dependently reversed the decline of percentage of cell survival in METH-treated SH-SY5Y cells, compared to the control group (Fig. 5A; $p < 0.001$). METH substantially increased the number of PI-positive dead cells, compared to the control group (Fig. 5B; $p < 0.001$). U73122 significantly decreased

the ratio of FDA-positive live/total cells, following METH exposure (Fig. 5B; $p < 0.001$). Treatment with siRNA-PLCβ1 significantly decreased 2.0 mM METH-induced apoptosis rate from 8.505% to 3.413% in SH-SY5Y cells (Fig. 5C; $p< 0.001$). There were no significant differences between the siRNA-NC+METH and METH groups ($p > 0.05$). One-way ANOVA analysis indicated that there was a significant group effect on ROS levels ($F_{(2, 6)} = 11.61$, $p < 0.01$). Further *post hoc* tests indicated that ROS levels in METH group were significantly higher than that of the control (Fig. 5D;$p < 0.01$) and METH+U73122 (Fig.5D; $p < 0.05$) groups. As shown in Fig. 5E, GRP78 protein expression of METH group was significantly higher than that of the control and METH+U73122 groups ($p < 0.01$).

Τηε εφφεςτ οφ ΠΛ˜β1 βλοςκαδε βψ Υ73122 ον τηε ΠΛ˜β1/ΠΚά/ ˜ΡΕΒ αςτιιτψ ιν ΜΕΤΗ-τρεατεδ ΣΗ-ΣΨ5Ψ ςελλς

As shown in Fig. 6, one-way ANOVA revealed that there was a significant group effect on PLCβ1, PKCα, and CREB protein expression in METH-treated SH-SY5Y cells (PLCβ1: $F_{(4, 10)} = 3083$, $p< 0.001$; PKCα: $F_{(4, 10)} = 827.8$, $p< 0.001$; CREB: $F_{(4, 10)} = 37.52$, $p< 0.001$). *Post hoc* analysis revealed that METH significantly increased PLCβ1, PKCα, and CREB protein and mRNA expression in SH-SY5Y cells, compared to the control group (PLCβ1:$p < 0.001$; PKCα, $p < 0.001$; CREB:$p < 0.001$; PLCβ1 mRNA: $p < 0.001$; PKCα mRNA, $p < 0.01$; CREB mRNA: $p < 0.01$). Treatment of 1.0, 3.0 and 10.0 μM U73122 significantly decreased PLCβ1, PKCα, and CREB protein expression in METH-treated cells, in comparison with METH group ($p < 0.001$). Treatment of 3.0 and 10.0 μM U73122 significantly decreased PLCβ1, PKCα, and CREB mRNA expression in METH-treated cells, in comparison with METH group ($p< 0.01$).

Τηε εφφεςτ οφ ΠΛ˜β1 βλοςκαδε βψ Υ73122 ον σψναπτις πλαστιςιτψ ςηανγες ιν ΜΕΤΗ-τρεατεδ ρατς

One-way analysis also indicated that there was significant group effect on both SYP ($F_{(2, 15)} = 7.676$, $p< 0.01$) and PSD-95 levels ($F_{(2, 15)} = 18.48$, $p < 0.001$). Further *post hoc* tests revealed that both SYP and PSD-95 protein expression of METH group was significantly greater than that of the control and METH+U73122 groups in PFC of METH-treated rats (Fig. 7A-C; $p < 0.01$).

Τηε εφφεςτ οφ ΠΛ˜β1 βλοςκαδε βψ Υ73122 ον ΜΕΤΗ ΣΑ ανδ ςυε-/δρυγ-ινδυςεδ ΜΕΤΗ ΣΑ ρεινςτατεμεντ.

Two-way ANOVA revealed that there were significant group (Fig. 8B;$F_{(2, 68)} = 7.634$, $p < 0.001$), dose (Fig. 8B; $F_{(3, 68)} = 170.8$, $p< 0.001$), and group × dose interaction (Fig. 8B;$F_{(6, 68)} = 2.454$, $p < 0.05$) effects on METH SA under the FR1 schedule. Increasing the METH dose significantly decreased METH consumption in all three groups. METH+10U73122 group earned significantly fewer infusions at both 25 and 50 μg/kg/infusion METH under the FR1 schedule, compared to METH+saline group (Fig. 8B; $p < 0.01$). In contrast, METH+5U73122 group only earned significantly fewer infusions of 50μg/kg/infusion METH under FR1 schedule than METH+saline group (Fig. 8B; $p < 0.01$). However, the differences for 75 and 100 μg/kg/infusion of METH failed to reach significance among three groups (Fig. 8B; $p > 0.05$). As shown in Fig. 8C, there were major group (Fig. 8C; $F_{(2, 52)} = 19.014$, $p < 0.001$), dose (Fig. 8C;$F_{(3, 52)} = 72.12$, $p < 0.001$) and group x dose interaction (Fig. 8C; $F_{(6, 52)} = 2.500$, $p < 0.05$) effects of U73122 on METH SA under PR schedule. Increasing the METH dose significantly increased the breakpoints for all three groups. Further *post hoc* analysis indicated that METH+10U73312 group produced significantly lower breakpoints compared to METH+saline group at both 50 and 100 μg/kg/infusion METH (Fig. 8C; 50 μg/kg/infusion,$p < 0.01$; 100 μg/kg/infusion, $p < 0.001$). METH+3U73122 group exhibited significantly fewer breakpoints than METH+saline group at 100 μg/kg/infusion METH dose (Fig. 8C;$p < 0.01$). However, there was no major effect of U73122 on METH SA maintained by 25 and 75 μg/kg/infusion METH under PR schedule.

For both cue- and drug-induced reinstatement of METH SA, one-way ANOVA analysis revealed that there was a major group effect on the number of active poking responses (Fig. 8D,$F_{(2, 12)} = 7.248$, $p < 0.01$; Fig. 8E, $F_{(2, 12)} = 14.42$, $p <0.001$). Compared to METH+saline group, the number of active poking responses significantly decreased in METH+3U37122 (Fig. 8D, $p< 0.05$) and METH+10U73122 (Fig. 8D,

$p< 0.05$) groups during the session of cue-induced reinstatement of METH SA. The similar effect of U73122 on drug-induced METH SA reinstatement is shown in Fig. 8E (3.0 mg/kg: $p < 0.01$; 10.0 mg/kg, $p < 0.001$). There were no significant differences in inactive poking responses among all the testing groups (Fig. 8D,$F_{(2, 12)} = 1.430$, $p = 0.2774$; Fig. 8E,$F_{(2, 12)} = 0.2500$, $p = 0.7828$).

Discussion

The present study demonstrated that PLCβ1-PKCα-CREB signaling pathway played an important role in the inhibitory effect of ATR1 on various METH-mediated behavioral effects. Firstly, ATR1 inhibition by CAN significantly elevated METH-induced behavioral dysfunction and neurotoxicity associated with increased oxidative stress. Furthermore, the data revealed that PLCβ1-PKCα-CREB signaling pathway, as well as a more specific role of PLCβ1, involved the inhibitory effects of AT1R on METH-induced behavioral dysfunction and neurotoxicity. Blockade of PLCβ1 by U73211 produced a significant effect on the reinforcing and motivation effects of METH, using the animal model of METH SA and drug/cue-induced reinstatement of METH SA.

The present study firstly examined the role of AT1R blockade by CAN on several behavioral effects of METH. CAN dose-dependently reversed the increased body temperature and locomotor activity induced by METH. Using the animal model of NOR and MWM, our study extended previous findings by demonstrating that AT1R inhibition by CAN could alleviate METH-induced learning and memory deficits(Li et al., 2014; Trofimiuk, Wielgat & Braszko, 2018). In comparison with the body temperature and locomotor activity testing data, the lower CAN dose (5 mg/kg) had a less substantial effect on NOR or MWM performance in METH-treated rats. In contrast, 10 mg/kg CAN completely restored the visual memory impairment, spatial learning, and memory deficits induced by METH. It should be noted that higher dose CAN treatment failed to alter the behavioral responses *per se* in rats, indicating the modulatory role of AT1R in the behavioral effect of METH. Cell death in various brain regions, including the cortex, Hip, and basal ganglia, has been suggested to characterize neurotoxicity that contributes cognitive function deficits (Zhang, Fu, Geng, Yang & Sun, 2012). Due to the tight link between neuronal toxicity and cognitive deficits, it was reasonably speculated that CAN decreased PFC and Hip apoptosis in METH-treated rats that exhibited cognitive deficits. Indeed, apoptotic cells were significantly increased in the PFC and Hip of METH-treated rats and cell viability was largely reduced differentiated PC12 cells. CAN pretreatment not only decreased apoptosis in the PFC and Hip of METH-treated rats, but also increased PC12 cell viability affected by METH. The study further investigated whether CAN exerted such beneficial effects via the altered level of Ang II and oxidative stress in the brain of METH-treated rats. Notably, CAN pretreatment significantly attenuated the augmented Ang II, MDA, NO, and NADPH levels in METH-treated rats. Furthermore, 10 mg/kg CAN reversed the decreased level of GSH-Px and SOD in METH-treated rats. Many studies have demonstrated that intracellular ROS attributes apoptotic cell death and excessive ROS release produces oxidative damage by lipid peroxidation (Wang et al., 2016). The results also showed that 10 μM CAN treatment significantly decreased METH-induced ROS formation in cells. This phenomenon may be partly due to the antioxidative ability of CAN. This eventuality is consistent with another study that showed CAN ameliorates pro-oxidative and pro-inflammatory markers in substantia nigra (SN) of aged rats(Diaz-Ruiz, Villar-Cheda, Dominguez-Meijide, Garrido-Gil, Guerra & Labandeira-Garcia, 2020). Our current studies demonstrated that decreased oxidative stress could be a major mechanism underlying the protective effects CAN on METH-induced neurotoxicity that is likely to result in cognitive deficits in rats.

Our previously published studies have demonstrated that PLCβ1 is associated with the protective effects of CAN in METH-induced behavioral deficits and neurotoxicity. The present study further explored the potential link between AT1R and METH-mediated behavioral effects via PLCβ1 regulation. In the current study, rats received either passive injections or produced voluntary behavioral of METH consumption. It was evident that PLCβ1 protein expression was specifically upregulated in the PFC and Hip of rats receiving daily passive injections of METH. In comparison with the sham group, PLCβ1 protein expression was obviously increased in the PFC, NAc, and Hip of METH SA rats under both FR1 and PR schedules. It is likely that the alteration of PLCβ1 was parallel with both the pharmacologic and reinforcing effects of METH. In

addition, the METH-mediated induction of PLCβ1 protein and mRNA expression occurred in SH-SY5Ycell in a dose- and time-dependent manner. Considering these findings, it is assumed that PLCβ1 may play an essential role to modulate the inhibition of Ang II on METH-induced behavioral effects. In the light of the altered expression of PLCβ1 in both METH-treated rats and cells, the present studies examined whether the inhibition of PLCβ1 enabled to alter neurotoxic effects of METH. The treatment of both PLCβ1 inhibitor, U73122, and SiRNA-PLCβ1 reversed the reduced cell viability and survival in SH-SY5Y cells treated with METH respectively. Mu-opioid receptor (MOR)-induced activation of PLCβ regulates PKC and subsequent ROS activity (Rodriguez-Munoz & Garzon, 2013). Administration of the PLC inhibitor U73122, as well as of the PKC inhibitors calphostin C and chelerythrine, dose-dependently reduce the immobility time in the forced swimming test by producing an antidepressant-like behavior (Galeotti & Ghelardini, 2011). Here, U73122 suppressed ROS production in SH-SY5Y cells and METH-induced ER stress through reduced GRP78. It was concluded that PLCβ1 effectively reduced excessive or accumulated ROS level that was associated with SH-SY5Y cells apoptosis induced by METH.

The role of signaling pathway of PLCβ1-PKC and CREB in METH effect was subsequently characterized. METH treatment upregulated the mRNA and protein expression of PLCβ1, PKCα, and CREB in SH-SY5Y cells and the NAc of rats that self-administered METH under FR1 schedule (Supplementary Figure S1). U73122 decreased CREB transcriptional activity and protein expression in a PLCβ1- and PKCα-dependent manner in SH-SY5Y cells. Ang II stimulation of renin may be mediated by PKCα-dependent augmentation of cAMP and CREB phosphorylation (Gonzalez et al., 2015). Previous studies have also shown that intracellular PLC signaling plays an important role in motor skill learning and associated cortical synaptic plasticity (Rioult-Pedotti, Pekanovic, Atiemo, Marshall & Luft, 2015). PLCβ1 in the CNS seems to be involved in numerous synaptic plasticity pathways in different diseases (Ratti et al., 2017). Therefore, we evaluated the expression of key synaptic proteins, SYP and PSD-95, in PFC. SYP and PSD-95 protein expression were significantly decreased in METH-treated rats. In contrast, U73122 administration counteracted the effects of METH and increased SYP and PSD95 protein levels in the PFC. Furthermore, U73122 prevented the expression of downstream enzyme of mGluR (mGluR1 and mGluR5) that mediated the effects of synaptic plasticity(Chen, Hu, Jiang, Potegal & Li, 2017). Taken together, the results suggest that PLCβ1-PKC-CREB signaling pathway might play important roles in the changes of synaptic plasticity that associated with METH-induced cognitive deficits. Previous evidence has shown that the AT1R-PLCβ-CREB signaling pathway may increase Ca^{2+}in the ER, a phenomenon that may lead to ER stress (Xu et al., 2019). Further research is needed to determine the role of Ang II in ER stress.

The present study is the first to demonstrate the role of PLCβ1 in METH SA and drug-/cue-induced reinstatement in rats. Administration of U73122 at 3 or 10 mg/kg significantly affected the response maintained on FR1 schedule and breakpoints obtained under PR schedule. Both cue- and drug-induced reinstatement of METH SA were suppressed by 3 and 10 mg/kg U73122 administration. Notably, inactive responses on the PR schedule and drug-induced seeking behavior were not significantly changed. In conclusion, U73122 effectively decreased METH SA under the FR1/PR schedule and reduced cue-/drug-seeking behavior after abstinence. CREB is a major transcriptional factor in the orchestration of synaptic plasticity and METH dependence. It is likely that the inhibitory effect of U73122 on the reinforcing and motivational effects of METH was via altered CREB activity.

In conclusion, our findings reveal an unappreciated role of the brain RAS with regard to alleviating a multitude of effects produced by METH. Our data may provide a potential therapeutic target for METH addition.

Author contributions

X.X. and Y.L. designed the study and prepared the manuscript; X.X., R.F., Y.R., M. X., J.H. performed all the in vivo and vitro experiments studies; M.C., X.L. participated in the analysis of the experiments. W.Z. and Y.L. contributed to the experimental design and revised the manuscript. All authors read and approved the final version of the manuscript.

Acknowledgments

Funding: This work was supported in part by the National Natural Science Foundation of China (81671323; 81971247), Zhejiang Provincial Key R & D Plan 2019 (2020C03064), Ningbo R & D Plan (20181ZDYF020172), National Social Science Foundation Key Programs (18ZDA215), and the Program for Innovative Research Team in Ningbo City (2015C110026).

Conflict of interest: The authors declare no conflicts of interest.

References

Alaei H, & Hosseini M (2007). Angiotensin converting enzyme inhibitor captopril modifies conditioned place preference induced by morphine and morphine withdrawal signs in rats. Pathophysiology 14**:** 55-60.

Bali A, & Jaggi AS (2013). Angiotensin as stress mediator: role of its receptor and interrelationships among other stress mediators and receptors. Pharmacological research 76**:** 49-57.

Bernheim A, See RE, & Reichel CM (2016). Chronic methamphetamine self-administration disrupts cortical control of cognition. Neurosci Biobehav Rev 69**:** 36-48.

Chen A, Hu WW, Jiang XL, Potegal M, & Li H (2017). Molecular mechanisms of group I metabotropic glutamate receptor mediated LTP and LTD in basolateral amygdala in vitro. Psychopharmacology (Berl) 234**:**681-694.

Dai M, Yang J, Xie M, Lin J, Luo M, Hua H*, et al.* (2017). Inhibition of JNK signalling mediates PPARalpha-dependent protection against intrahepatic cholestasis by fenofibrate. British journal of pharmacology 174**:** 3000-3017.

Darke S, Kaye S, McKetin R, & Duflou J (2008). Major physical and psychological harms of methamphetamine use. Drug Alcohol Rev 27**:** 253-262.

Diaz-Ruiz C, Villar-Cheda B, Dominguez-Meijide A, Garrido-Gil P, Guerra MJ, & Labandeira-Garcia JL (2020). Aging-Related Overactivity of the Angiotensin/AT1 Axis Decreases Sirtuin 3 Levels in the Substantia Nigra, Which Induces Vulnerability to Oxidative Stress and Neurodegeneration. J Gerontol A Biol Sci Med Sci 75**:** 416-424.

Galeotti N, & Ghelardini C (2011). Antidepressant phenotype by inhibiting the phospholipase Cbeta(1)–protein kinase Cgamma pathway in the forced swim test. Neuropharmacology 60**:** 937-943.

Gonzalez AA, Liu L, Lara LS, Bourgeois CR, Ibaceta-Gonzalez C, Salinas-Parra N*, et al.* (2015). PKC-alpha-dependent augmentation of cAMP and CREB phosphorylation mediates the angiotensin II stimulation of renin in the collecting duct. American journal of physiology Renal physiology 309**:** F880-888.

Hariharan A, Shetty S, Shirole T, & Jagtap AG (2014). Potential of protease inhibitor in 3-nitropropionic acid induced Huntington's disease like symptoms: mitochondrial dysfunction and neurodegeneration. Neurotoxicology 45**:** 139-148.

Hartel-Petri R, Krampe-Scheidler A, Braunwarth WD, Havemann-Reinecke U, Jeschke P, Looser W*, et al.* (2017). Evidence-Based Guidelines for the Pharmacologic Management of Methamphetamine Dependence, Relapse Prevention, Chronic Methamphetamine-Related, and Comorbid Psychiatric Disorders in Post-Acute Settings. Pharmacopsychiatry 50**:**96-104.

Henry BL, Minassian A, & Perry W (2010). Effect of methamphetamine dependence on everyday functional ability. Addict Behav 35**:**593-598.

Ivanova N, & Tchekalarova J (2019). The Potential Therapeutic Capacity of Inhibiting the Brain Renin-Angiotensin System in the Treatment of Co-Morbid Conditions in Epilepsy. CNS Drugs 33**:** 1101-1112.

Jiang L, Huang M, Xu S, Wang Y, An P, Feng C*, et al.* (2016). Bis(propyl)-cognitin Prevents beta-amyloid-induced Memory Deficits as Well as Synaptic Formation and Plasticity Impairments via the Activation of PI3-K Pathway. Molecular neurobiology 53**:** 3832-3841.

Jiang L, Zhu R, Bu Q, Li Y, Shao X, Gu H*, et al.* (2018). Brain Renin-Angiotensin System Blockade Attenuates Methamphetamine-Induced Hyperlocomotion and Neurotoxicity. Neurotherapeutics 15**:**500-510.

Kehoe PG, Al Mulhim N, Zetterberg H, Blennow K, & Miners JS (2019). Cerebrospinal Fluid Changes in the Renin-Angiotensin System in Alzheimer's Disease. J Alzheimers Dis 72**:** 525-535.

Krasniqi S, & Daci A (2019). Role of the Angiotensin Pathway and its Target Therapy in Epilepsy Management. International journal of molecular sciences 20.

Labandeira-Garcia JL, Rodriguez-Perez AI, Garrido-Gil P, Rodriguez-Pallares J, Lanciego JL, & Guerra MJ (2017). Brain Renin-Angiotensin System and Microglial Polarization: Implications for Aging and Neurodegeneration. Front Aging Neurosci 9**:** 129.

Labandeira-Garcia JL, Rodriguez-Perez AI, Valenzuela R, Costa-Besada MA, & Guerra MJ (2016). Menopause and Parkinson's disease. Interaction between estrogens and brain renin-angiotensin system in dopaminergic degeneration. Front Neuroendocrinol 43**:** 44-59.

Lecomte T, Dumais A, Dugre JR, & Potvin S (2018). The prevalence of substance-induced psychotic disorder in methamphetamine misusers: A meta-analysis. Psychiatry Res 268**:** 189-192.

Li X, Li S, Zheng W, Pan J, Huang K, Chen R*, et al.* (2015). Environmental enrichment and abstinence attenuate ketamine-induced cardiac and renal toxicity. Scientific reports 5**:** 11611.

Li Z, Cao Y, Li L, Liang Y, Tian X, Mo N*, et al.* (2014). Prophylactic angiotensin type 1 receptor antagonism confers neuroprotection in an aged rat model of postoperative cognitive dysfunction. Biochemical and biophysical research communications 449**:** 74-80.

Ma J, Li XD, Wang TY, Li SX, Meng SQ, Blow FC*, et al.* (2018). Relationship between the duration of methamphetamine use and psychotic symptoms: A two-year prospective cohort study. Drug Alcohol Depend 187**:** 363-369.

Marchese NA, Artur de laVillarmois E, Basmadjian OM, Perez MF, Baiardi G, & Bregonzio C (2016). Brain Angiotensin II AT1 receptors are involved in the acute and long-term amphetamine-induced neurocognitive alterations. Psychopharmacology (Berl) 233**:** 795-807.

Marchese NA, Occhieppo VB, Basmadjian OM, Casarsa BS, Baiardi G, & Bregonzio C (2019). Angiotensin II modulates amphetamine-induced glial and brain vascular responses, and attention deficit via angiotensin type 1 receptor: Evidence from brain regional sensitivity to amphetamine. The European journal of neuroscience.

Mark KA, Soghomonian JJ, & Yamamoto BK (2004). High-dose methamphetamine acutely activates the striatonigral pathway to increase striatal glutamate and mediate long-term dopamine toxicity. The Journal of neuroscience : the official journal of the Society for Neuroscience 24**:** 11449-11456.

McKetin R, Hides L, Kavanagh DJ, Saunders JB, & Dawe S (2018). First psychotic episode risk markers for primary psychosis amongst people who use methamphetamine. Schizophr Res 199**:** 456-457.

Moszczynska A, & Callan SP (2017). Molecular, Behavioral, and Physiological Consequences of Methamphetamine Neurotoxicity: Implications for Treatment. The Journal of pharmacology and experimental therapeutics 362**:** 474-488.

Newton TF, Kalechstein AD, Duran S, Vansluis N, & Ling W (2004). Methamphetamine abstinence syndrome: preliminary findings. Am J Addict 13**:** 248-255.

Potvin S, Pelletier J, Grot S, Hebert C, Barr AM, & Lecomte T (2018). Cognitive deficits in individuals with methamphetamine use disorder: A meta-analysis. Addict Behav 80**:** 154-160.

Ratti S, Mongiorgi S, Ramazzotti G, Follo MY, Mariani GA, Suh PG, *et al.* (2017). Nuclear Inositide Signaling Via Phospholipase C. Journal of cellular biochemistry 118**:** 1969-1978.

Rendell PG, Mazur M, & Henry JD (2009). Prospective memory impairment in former users of methamphetamine. Psychopharmacology (Berl) 203**:** 609-616.

Rioult-Pedotti MS, Pekanovic A, Atiemo CO, Marshall J, & Luft AR (2015). Dopamine Promotes Motor Cortex Plasticity and Motor Skill Learning via PLC Activation. PloS one 10**:** e0124986.

Rodriguez-Munoz M, & Garzon J (2013). Nitric oxide and zinc-mediated protein assemblies involved in mu opioid receptor signaling. Molecular neurobiology 48**:** 769-782.

Rogers JL, De Santis S, & See RE (2008). Extended methamphetamine self-administration enhances reinstatement of drug seeking and impairs novel object recognition in rats. Psychopharmacology (Berl) 199**:** 615-624.

Royea J, Zhang L, Tong XK, & Hamel E (2017). Angiotensin IV Receptors Mediate the Cognitive and Cerebrovascular Benefits of Losartan in a Mouse Model of Alzheimer's Disease. The Journal of neuroscience : the official journal of the Society for Neuroscience 37**:** 5562-5573.

Sharifi F, Reisi P, & Malek M (2019). Angiotensin 1 receptor antagonist attenuates acute kidney injury-induced cognitive impairment and synaptic plasticity via modulating hippocampal oxidative stress. Life sciences 234**:** 116775.

Simon SL, Domier C, Carnell J, Brethen P, Rawson R, & Ling W (2000). Cognitive impairment in individuals currently using methamphetamine. Am J Addict 9**:** 222-231.

Simon SL, Domier CP, Sim T, Richardson K, Rawson RA, & Ling W (2002). Cognitive performance of current methamphetamine and cocaine abusers. J Addict Dis 21**:** 61-74.

Soares E, & Pereira FC (2019). Pharmacotherapeutic strategies for methamphetamine use disorder: mind the subgroups. Expert Opin Pharmacother 20**:** 2273-2293.

Tata DA, & Yamamoto BK (2008). Chronic stress enhances methamphetamine-induced extracellular glutamate and excitotoxicity in the rat striatum. Synapse (New York, NY) 62**:** 325-336.

Trofimiuk E, Wielgat P, & Braszko JJ (2018). Candesartan, angiotensin II type 1 receptor blocker is able to relieve age-related cognitive impairment. Pharmacol Rep 70**:** 87-92.

Veerasakul S, Thanoi S, Reynolds GP, & Nudmamud-Thanoi S (2016). Effect of Methamphetamine Exposure on Expression of Calcium Binding Proteins in Rat Frontal Cortex and Hippocampus. Neurotox Res 30**:** 427-433.

Vian J, Pereira C, Chavarria V, Kohler C, Stubbs B, Quevedo J, *et al.* (2017). The renin-angiotensin system: a possible new target for depression. BMC Med 15**:** 144.

Visniauskas B, Perry JC, Oliveira V, Dalio FM, Andersen ML, Tufik S, *et al.* (2012). Cocaine administration increases angiotensin I-converting enzyme (ACE) expression and activity in the rat striatum and frontal cortex. Neuroscience letters 506**:** 84-88.

Wang J, Zheng J, Huang C, Zhao J, Lin J, Zhou X, *et al.* (2018). Eckmaxol, a Phlorotannin Extracted from Ecklonia maxima, Produces Anti-beta-amyloid Oligomer Neuroprotective Effects Possibly via Directly Acting on Glycogen Synthase Kinase 3beta. ACS Chem Neurosci 9**:**1349-1356.

Wang X, Miao J, Yan C, Ge R, Liang T, Liu E, *et al.* (2016). Chitosan attenuates dibutyltin-induced apoptosis in PC12 cells through inhibition of the mitochondria-dependent pathway. Carbohydr Polym 151**:** 996-1005.

Wright JW, & Harding JW (2019). Contributions by the Brain Renin-Angiotensin System to Memory, Cognition, and Alzheimer's Disease. J Alzheimers Dis 67**:** 469-480.

Wright JW, Yamamoto BJ, & Harding JW (2008). Angiotensin receptor subtype mediated physiologies and behaviors: new discoveries and clinical targets. Prog Neurobiol 84**:** 157-181.

Xu X, Pan J, Li X, Cui Y, Mao Z, Wu B*, et al.* (2019). Inhibition of Methamphetamine Self-Administration and Reinstatement by Central Blockade of Angiotensin II Receptor in Rats. The Journal of pharmacology and experimental therapeutics 369**:** 244-258.

Zhang P, Pan J, Mao Z, Xu X, Lin D, Wu B*, et al.* (2019). The effects of early exposure to MK-801 during environmental enrichment on spatial memory, methamphetamine self-administration and cue-induced renewal in rats. Behav Brain Res 363**:** 83-93.

Zhang TL, Fu JL, Geng Z, Yang JJ, & Sun XJ (2012). The neuroprotective effect of losartan through inhibiting AT1/ASK1/MKK4/JNK3 pathway following cerebral I/R in rat hippocampal CA1 region. CNS Neurosci Ther 18**:** 981-987.

Zhong N, Jiang H, Du J, Zhao Y, Sun H, Xu D*, et al.* (2016). The cognitive impairments and psychological wellbeing of methamphetamine dependent patients compared with health controls. Prog Neuropsychopharmacol Biol Psychiatry 69**:** 31-37.

Zhu JP, Xu W, & Angulo JA (2006). Methamphetamine-induced cell death: selective vulnerability in neuronal subpopulations of the striatum in mice. Neuroscience 140**:** 607-622.

Figures and figure legends:

Fig. 1. Effects of candesartan cilexetil (CAN) on methamphetamine (METH)-induced body temperature, behavioral sensitization, cognitive impairments, and learning and memory deficits in rats. (A) Timeline of the experimental procedures. **(B)** Body temperatures of adult male SD rats administered METH (10.0 mg/kg) and CAN (5.0 or 10.0 mg/kg). Data are expressed as change in temperature (°C) from the Saline+DMSO group. $^{\#\#}p< 0.01$; METH+5CAN group and METH+10CAN group vs. METH+DMSO group. $^{**}p < 0.01$ and $^{***}p < 0.001$.**(C)** Effect of CAN on the locomotor activity test with METH. Each vertical line represents one METH infusion. Two-way analysis of variance (ANOVA) with repeated measures over time revealed a significant CAN treatment main effect ($F_{(4,\ 8)} = 2070$, $p < 0.001$, statistically significant difference across all treatment groups) and time effect ($F_{(3,\ 6)} = 4.78$, $p < 0.05$, statistically significant difference across all the time points).**(D)** CAN attenuated METH-induced cognitive impairments in rats. Quantitative comparison of the discrimination indexes of the object in the training session. The recognition index was not significantly altered among various groups (as indicated). Quantitative comparison of the recognition indexes in the retention session. CAN significantly attenuated the METH-mediated reduction of recognition index in rats ($^{\#\#\#}p < 0.001$ vs. the Saline+DMSO group, $^{**}p < 0.01$ vs. the METH+DMSO group, one-way ANOVA followed by Tukey's test). **(E)** Effects of CAN on METH-induced learning and memory deficits in a Morris water maze test in rats. $^{**}p < 0.01$, METH+10CAN group vs. the METH+DMSO group; $^{\#}p < 0.05$, METH+5CAN group vs. the METH+DMSO group. Data are expressed as the mean ± standard deviation (SD; treatment: $F_{(4,\ 12)} = 28.18$,$p < 0.001$; time: $F_{(3,\ 9)} = 121.6$, $p < 0.001$; two-way repeated measures ANOVA with Bonferroni's post hoc tests).

Fig. 2. Effects of candesartan cilexetil (CAN) on methamphetamine (METH)-induced neurotoxicity and apoptosis in rats.(A-E) TUNEL+ cells (%) of the various groups and their corresponding control groups in the prefrontal cortex. Representative images of TUNEL staining for various groups. **(F)** Quantitative results showed that CAN prevents prefrontal cortex apoptotic responses in METH-induced rats. **(G-K)** Representative images of TUNEL staining in the hippocampal region in various groups as indicated**(L)** . The relative quantity analysis was showed that CAN decreased apoptosis in the hippocampal region of rats. METH+10CAN group vs. METH+DMSO group, $^{***}p < 0.001$; METH+5CAN group vs. METH+DMSO group, $^{***}p < 0.001$; METH+DMSO group vs. Saline+DMSO group, $^{\#\#\#}p < 0.001$ (one-way analysis of variance (ANOVA) and Tukey's test; scale bar: 30 μm). **(M)** AngII level, **(N)** malondialdehyde (MDA) expression, **(O)** nitric oxide (NO) expression, **(P)**nicotinamide adenine dinucleotide

phosphate (NADPH) expression,**(Q)** glutathione peroxidase (GSH-Px) expression, and**(I)** superoxide dismutase (SOD) expression were evaluated by enzyme-linked immunosorbent assay (ELISA) in the brain of rats.$^{\#\#}p < 0.01$,$^{\#\#\#}p < 0.001$ vs. control group, $^{*}p < 0.05$, $^{**}p < 0.01$, $^{***}p< 0.001$ vs. METH+DMSO group (one-way ANOVA and Tukey's test).

Fig. 3. Candesartan cilexetil (CAN) attenuated the methamphetamine (METH)-induced neurotoxic effects in PC12 cells.

(A) The neurotoxicity and apoptosis induced by METH were decreased by CAN in PC12 cells. **(B)** PC12 cells were treated with the 10.0 μM CAN and 2.0mM METH. After 24 h, cells were examined via fluorescein diacetate (FDA)/propidium iodide (PI) double staining.**(C)** CAN significantly protected against the METH-induced increase in intracellular ROS in PC12 cells. PC12 cells were treated with 10 μM CAN. After 2 h, cells were exposed to 2.5 mM METH. Intracellular ROS was measured by DCFH-DA assay at 2 h after METH treatment. Data are presented as the mean ± standard deviation (SD) of three separate experiments; $^{\#\#\#}p < 0.01$ vs. the control group, $^{***}p < 0.01$ vs. the METH-treated group (one-way analysis of variance [ANOVA] and Tukey's test).

Φιγ. 4. Τηε εφφεςτ οφ μετηαμπηεταμινε (METH) ον τηε εξπρεσσιον οφ ανγιοτενσιν II τψπε I ρεςεπτορ (AT1P) ανδ πηοσπηολιπασε ̃ β1 (ΠΛ̃β1) προτεινς ιν ιο ανδ ιν ιτρο. (A, B) Representative and quantitative western blot assay results of AT1R and PLCβ1. Protein expression was significantly upregulated in the prefrontal cortex (PFC) and hippocampus (Hip) of METH-exposed male SD rats, $^{**}p < 0.01$, $^{***}p < 0.001$.**(C)** Representative and quantitative western blot assays, illustrating that on the fixed ration 1 (FR1) schedule of METH SA, the expression of PLCβ1 in the PFC, nucleus accumbens (NAc), and Hip were significantly increased; there was no change in the caudate putamen (CPu) of the rats, $^{**}p < 0.01$, $^{***}p < 0.001$. **(D, E)** Representative and quantitative western blot assays, illustrating that on the progressive ratio (PR) schedule of METH self-administration (SA), PLCβ1 expression in the PFC and Hip was significantly increased, $^{*}p < 0.05$, $^{**}p< 0.01$. **(G, I)** SH-SY5Y cells were treated with 1.0–3.0 mM METH for 24 h or with 2.0 mM METH for 2–24 hour as indicated. . **(F, H)**Representative and quantitative analyses were performed to determine PLCβ1 and CREB protein expression. Fold induction relative to vehicle-treated cells is shown. $^{*}p < 0.05$; $^{**}p< 0.01$, $^{***}p < 0.001$ vs. vehicle control group. Data were analyzed by one-way analysis of variance (ANOVA) followed by Fisher's least significant difference (LSD) *post hoc*analyses.

Φιγ. 5. Βλοςκαδε οφ τηε πηοσπηολιπασε ̃ β1 (ΠΛ̃β1) αττενυατεδ μετηαμπηεταμινε (METH)-ινδυςεδ ςελλ αποπτοσις ανδ οξιδατιε στρεσς ιν ΣΗ-ΣΨ5Ψ ςελλς. (A) Data are expressed as the percentage of control and presented as the mean ± standard deviation (SD) of three separate experiments; $^{\#\#}p < 0.01$ vs. the control group, $^{*}p < 0.05$, $^{**}p < 0.01$ vs. the METH-challenged group (one-way ANOVA and Tukey's test).**(B)** 3 μM U73122 prevented METH-induced cell death, as evidenced by fluorescein diacetate (FDA)/propidium iodide (PI) double staining in SH-SY5Y cells. Representative figures demonstrated FDA-positive viable neurons and PI-positive dead neurons in various groups as indicated.$^{\#\#\#}p < 0.01$ vs. the control group, $^{***}P < 0.01$ vs. the METH-challenged group (one-way analysis of variance (ANOVA) and Tukey's test). **(C)**Representative Annexin V/PI labeling, assessed by flow cytometry, was used to analyze the ratio of apoptotic SH-SY5Y cells. Data are expressed as the mean ± SD. Results were analyzed using one-way ANOVA; n = 4.$^{\#\#\#}p < 0.001$, METH group vs. control group; $^{***}p < 0.001$, siRNA-PLCβ1 group vs. siRNA-NC group. **(D)** The reactive oxygen species (ROS) level was measured by DCFH-DA staining and flow cytometry analysis following treatment with METH and U73122 in SH-SY5Y cells. Statistical graph of DCFH-DA green fluorescence-positive cells as the fold change compared to the control. $^{\#\#}p < 0.01$ vs. the control group, $^{*}p < 0.05$ vs. the METH group.**(E)** Representative green-fluorescence-positive cells (DCFH-DA positive cells) represent cells with ROS formation. **(F)** Western blot analysis revealed a strong upregulation of glucose-regulated protein 78 (GRP78), which is involved in ROS generation.

Φιγ. 6. Τηε εφφεςτ οφ πηοσπηολιπασε ̃ β1 (ΠΛ̃β1) βλοςκαδε βψ Υ73122 ον τηε ΠΛ̃β1/προτειν κινασε ̃ α (ΠΚα̃)/ςΑΜΠ ρεσπονσε ελεμεντ-βινδινγ προτειν (̃PEB) α-

στιιτψ ιν μετηαμπηεταμινε (METH)-τρεατεδ ΣΗ-ΣΨ5Ψ ςελλς . Western blotting analysis of PLCβ1, PKCα, and CREB protein expression in SH-SY5Y cells. Representative western blots **(A)** and quantitative data**(B, C, and D)** for the protein expression. Compared with the control group, PLCβ1, PKCα, and CREB were significantly increased in METH-treated group. Quantitative real-time polymerase chain reaction (qRT-PCR) was performed to determine PLCβ1 **(E)** ,PKCα**(F)** , and CREB **(G)** messenger RNA (mRNA) expression. Western blotting analysis of PLCβ1, PKCα, and CREB protein expression in SH-SY5Y cells. The expression of each was markedly increased by pretreatment with U73122 ($^{\#\#}p < 0.01$, $^{\#\#\#}p < 0.001$; $^{**}p < 0.01$, $^{***}p < 0.001$).

Φιγ. 7. Τηε εφφεςτ οφ πηοσπηολιπασε ˆ β1 (ΠΛˆβ1) βλοςκαδε βψ Υ73122 ον σψναπτις πλαστιςιτψ ςηανγες. Representative **(A)** and quantitative **(B, C)** Western blot analysis, illustrating that METH treatment significantly increased the expression of synaptophysin (SYP; **B** , $^{\#}p < 0.05$, METH group vs. control group) and post-synaptic density 95 (PSD-95;**C** , $^{\#\#\#}p < 0.001$, METH group vs. control group) in SH-SY5Y cells. This increase was attenuated by U73122 pretreatment. Each brain sample was replicated three times in western blot assays. $^{**}p < 0.01$, METH+U73122 group vs. METH group (one-way analysis of variance (ANOVA) and Tukey's test).

Fig. 8. The effects of U73122 on methamphetamine (METH) self-administration (SA), cue- and drug-induced METH-seeking in rats.(A) Timeline of the METH SA and cue- and drug-induced relapse experiments. **(B)** The effect of U73122 on METH SA under the fixed ratio 1 (FR1) schedule. Compared with the METH groups, the 3.0 and 10 mg/kg U73122 groups earned significantly fewer infusions of 25 and 50 μg/kg METH per infusion after METH SA under the FR1 schedule. $^{\#\#}p < 0.01$, 10 mg/kg U73122 vs. METH. $^{*}p < 0.05$, 3.0 mg/kg U73122 vs. METH.**(C)** The effect of U73122 on METH SA under the progressive ratio (PR) schedule. Increasing the METH dose significantly increased breakpoints for all groups. The METH group produced significantly higher breakpoints maintained by 25, 50, and 100 μg/kg per infusion METH compared to the 3.0 and 10 mg/kg U73122 groups.$^{\#}p < 0.05$,$^{\#\#}p < 0.01$,$^{\#\#\#}p < 0.001$, 10 mg/kg U73122 vs. METH. $^{*}p < 0.05$, $^{**}p < 0.01$, 3.0 mg/kg U73122 vs. METH. **(D)** the effect U73122 on cue-induced drug seeking in mice after 14 days of withdrawal from previous METH self-administration. $^{*}p < 0.05$, 3.0 or 10.0 mg/kg U73122 vs. METH group. **(E)** The effect of U73122 on drug-induced reinstatement of METH SA. The responses significantly decreased in the 3.0 mg/kg U73122 ($^{**}p < 0.01$) and 10.0 mg/kg U73122 ($^{***}p < 0.01$) groups compared to those in METH groups. Data are expressed as the mean ± standard deviation (SD).

Figrue 1

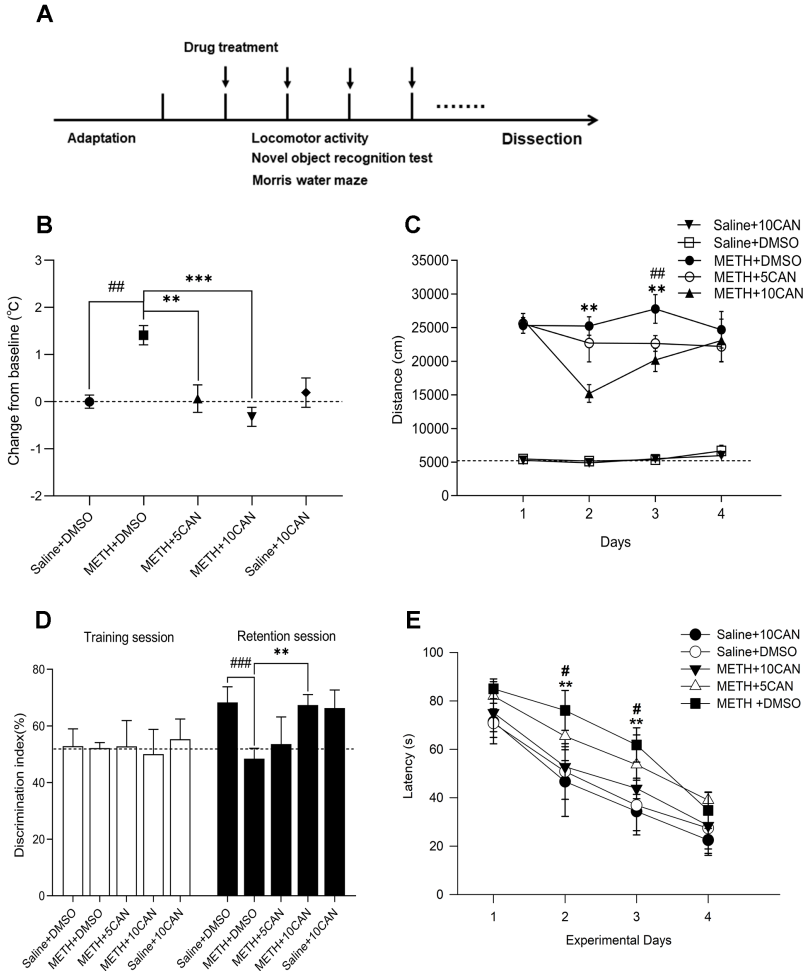

Figure 2

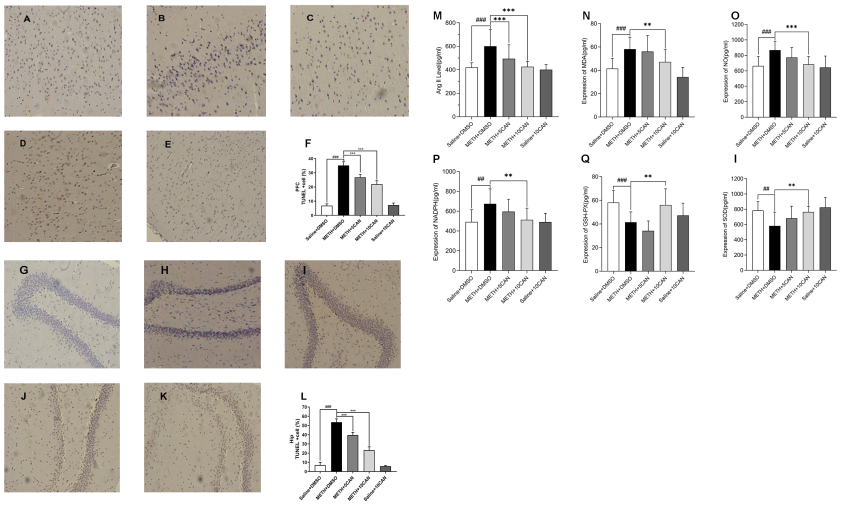

Figure 3

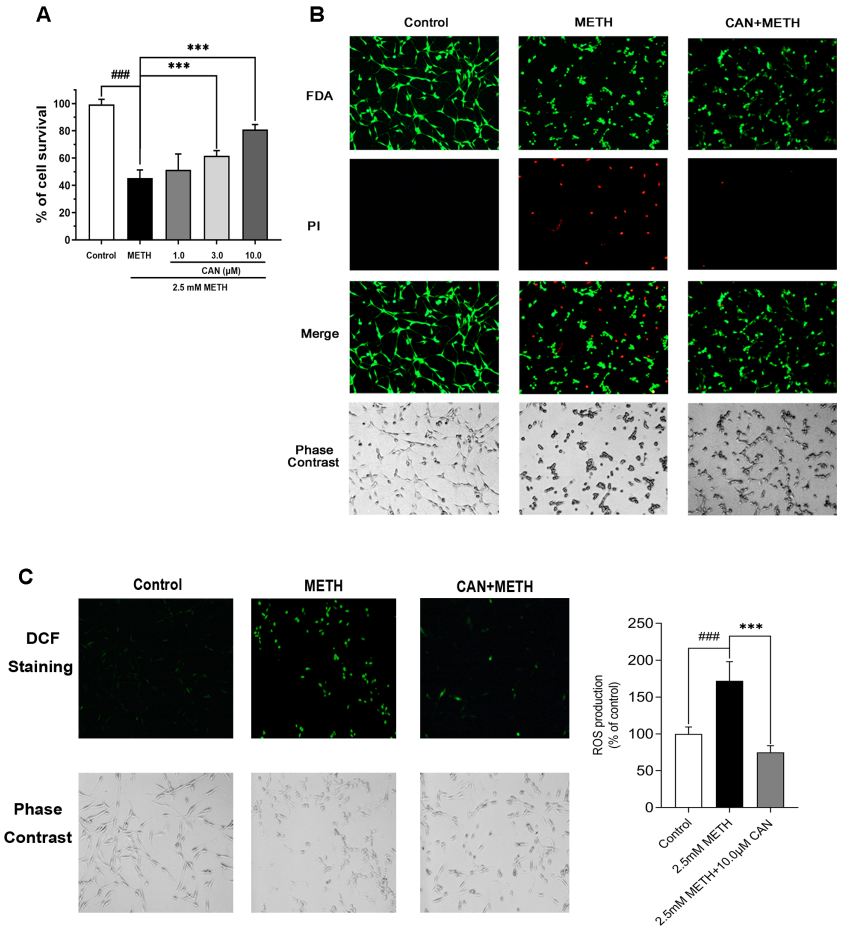

Figure 4

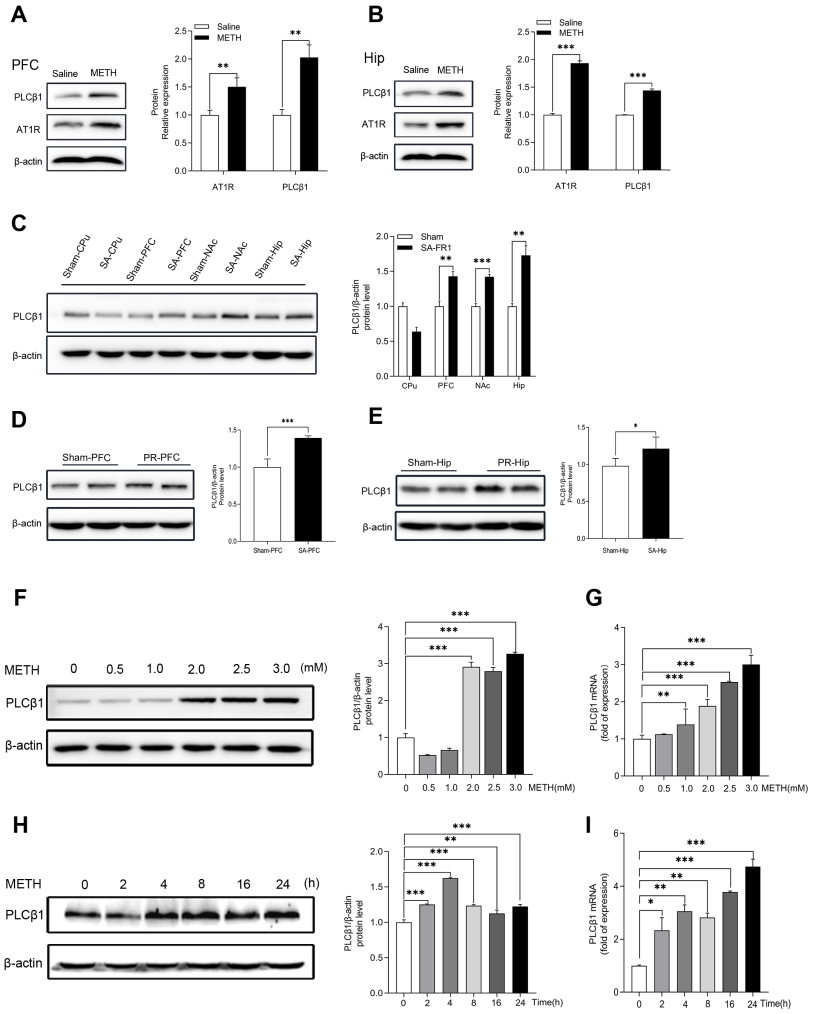

Figure 5

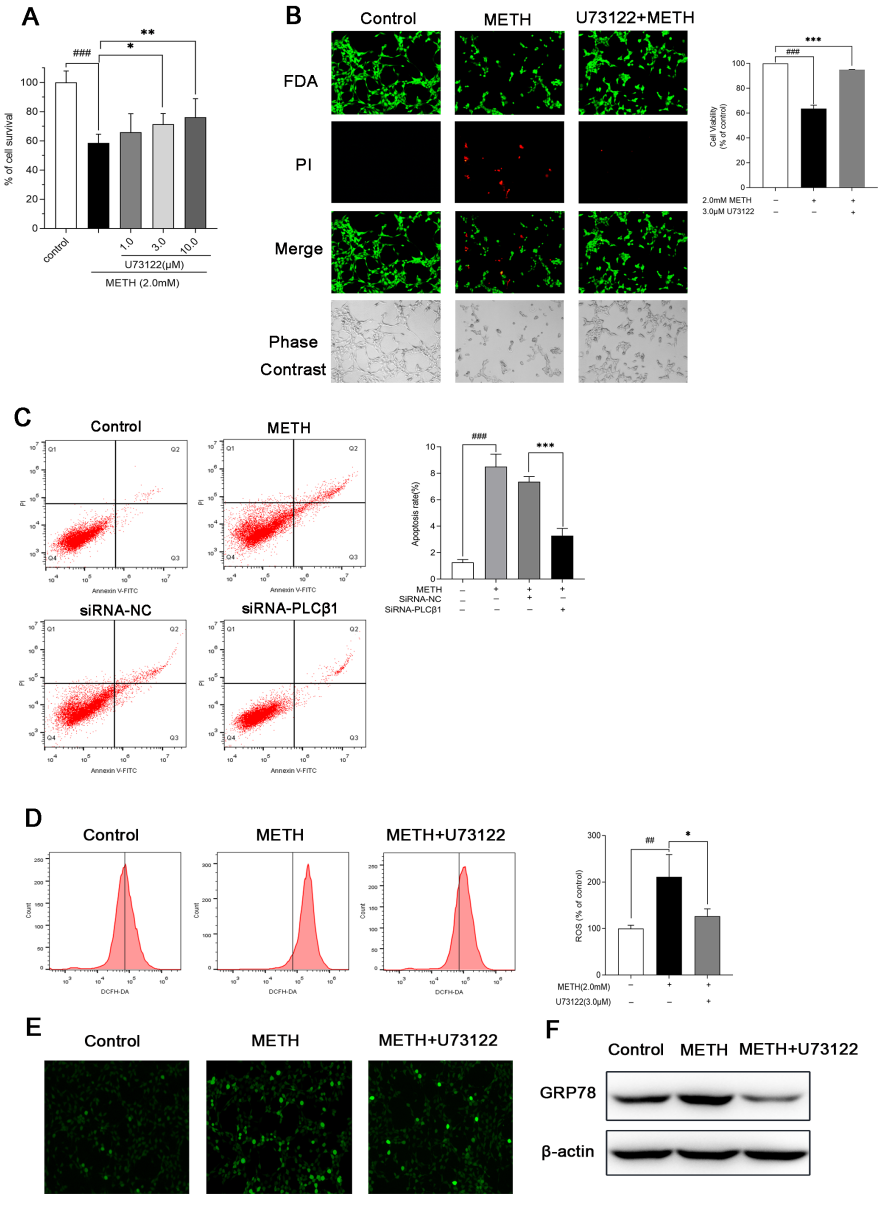

Figure 6

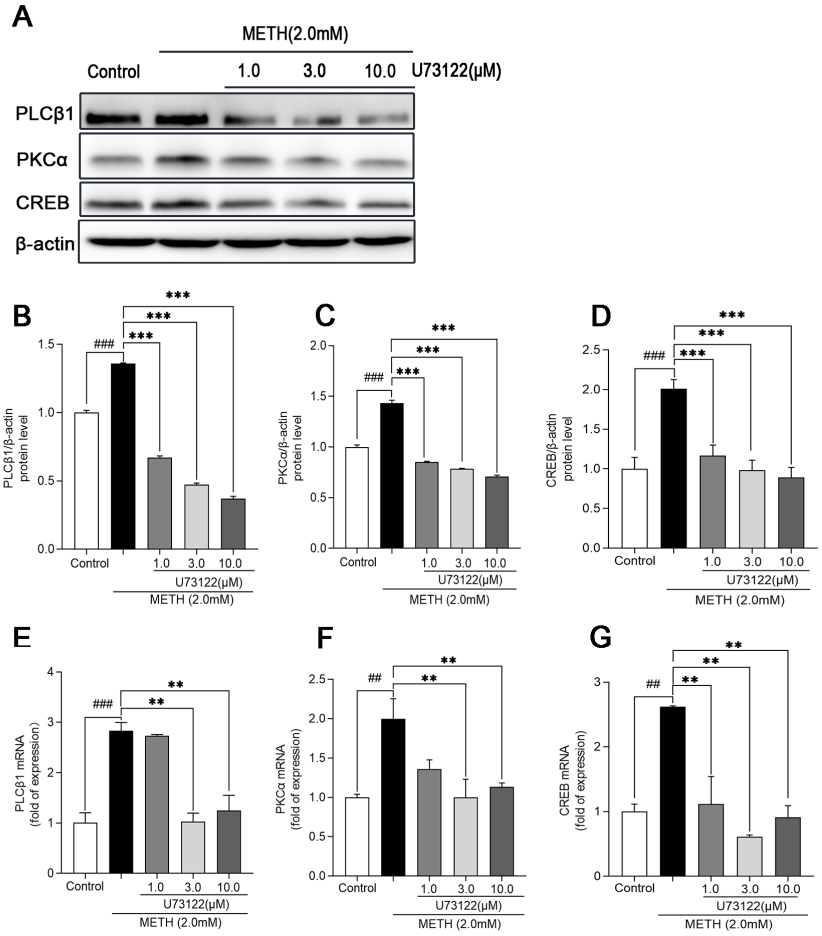

Figure 7

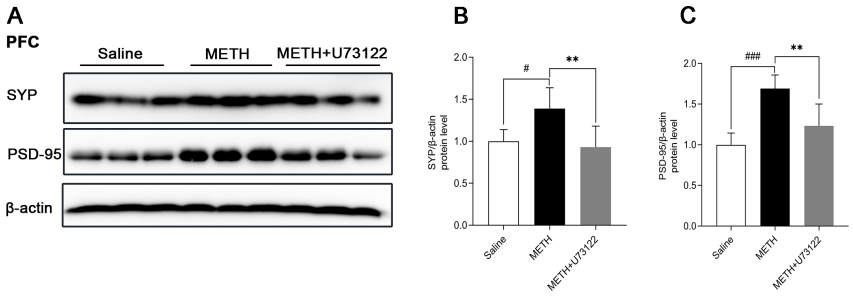

Figure 8